INSTITUTE OF PHYSICS PUBLISHING NANOTECHNOLOGY
Nanotechnology **17** (2006) 5781–5785 doi:10.1088/0957-4484/17/23/012

# Efficient photoinduced charge transfer in $TiO_2$ nanorod/conjugated polymer hybrid materials

**Yu-Ting Lin, Tsung-Wei Zeng, Wei-Zong Lai, Chun-Wei Chen[1], Yun-Yue Lin, Yu-Sheng Chang and Wei-Fang Su[1]**

Department of Materials Science and Engineering, National Taiwan University, Taipei, Taiwan

E-mail: chunwei@ntu.edu.tw and suwf@ntu.edu.tw

Received 23 September 2006, in final form 17 October 2006
Published 10 November 2006
Online at stacks.iop.org/Nano/17/5781

**Abstract**
The mechanisms of photoinduced charge transfer in composites of $TiO_2$ nanorods with a conjugated polymer (poly(2-methoxy-5-(2′-ethyl)(hexyloxy) 1,4-phenylenevinylene) (MEH-PPV) have been investigated by steady-state, time-resolved photoluminescence (PL) spectroscopy and photoluminescence excitation (PLE) spectroscopy. Efficient charge separation takes place at the $TiO_2$-nanorod/polymer interfaces when the polymer is excited, leading to quenching of the photoluminescence efficiency $\eta$ and shortening of the measured lifetime $\tau_{PL}$. In addition, the low-temperature absorption and photoluminescence spectra show that the inclusion of $TiO_2$ nanorods in polymer can reduce disorder in conformation and enhance conjugation in the polymer chain. A photovoltaic solar cell device based on the MEH-PPV/$TiO_2$-nanorod composite material is also presented, which shows a two order increase in short-circuit current $J_{SC}$ compared to that based on the pristine MEH-PPV.

(Some figures in this article are in colour only in the electronic version)

## 1. Introduction

Recently, composites of organic polymers and inorganic nanoparticles have attracted great interest due to their potential application in developing low-cost, large-area, mechanically flexible photovoltaic devices [1, 2]. A basic requirement for a photovoltaic material is to generate free charge carriers produced by photoexcitation. Subsequently, these carriers are transported through the device to the electrodes without recombining with oppositely charged carriers. Due to the low dielectric constant of organic materials, the dominant photogenerated species in most conjugated polymers is a neutral bound electron–hole pair (exciton). These neutral excitons can be dissociated from Coulomb attraction by offering an energetically favourable pathway for the electron from polymer (donor) to transfer to an electron-accepting species (acceptor). Charge separation in the polymer is often enhanced by inclusion of a high-electron-affinity substance such as the fullerene derivative [6,6]-phenyl-$C_{61}$ butyric acid methyl ester (PCBM) [3, 4], organic dyes [5, 6], or nanocrystals [1, 7]. Nanocrystals are considered to be more attractive in photovoltaic applications due to their large surface-to-bulk ratio, giving an extension of interfacial area for electron transfer, and higher stability. The charge separation process must be fast compared to radiative or non-radiative decays of the singlet exciton, leading to quenching of the photoluminescence (PL) intensities. However, electron transport in the polymer/nanoparticle hybrid is usually limited by poorly formed conduction path [7]. Thus, one-dimensional semiconductor nanorods are preferable over nanoparticles for offering direct pathways for electric conduction. It has been demonstrated that the solar cell based on the CdSe nanorod/poly(3-hexylthiophene) (P3HT) hybrid material exhibits better power conversion efficiency than its CdSe nanoparticle counterpart [1]. The environmentally friendly and low-cost $TiO_2$ nanocrystal is another promising material in hybrid polymer/nanocrystal solar cell applications [8, 9]. In this report, the microscopic mechanisms of photo-

[1] Authors to whom any correspondence should be addressed.

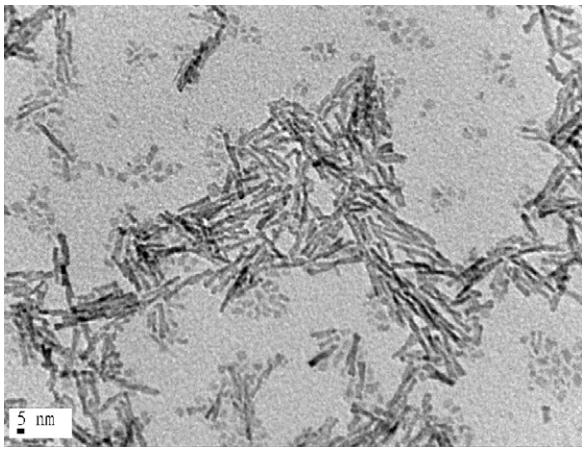


**Figure 1.** TEM image of $TiO_2$ nanorods with a size of 4–5 nm in diameter and 20–40 nm in length.

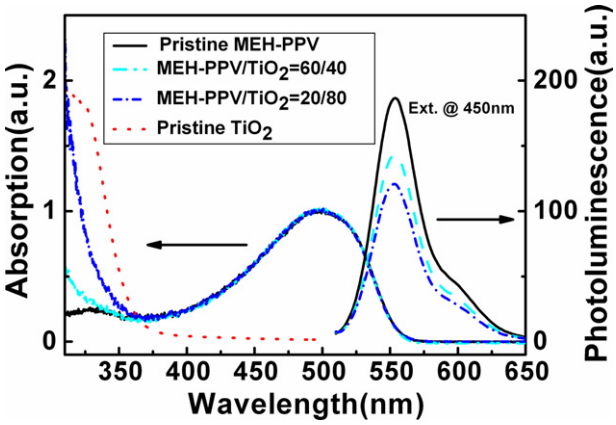


**Figure 2.** (a) Absorption and photoluminescence spectra of blends of MEH-PPV with $TiO_2$ nanorods for increasing concentrations of $TiO_2$ nanorods: (a) 0 wt%, (b) 40 wt%, (c) 80 wt%. (d) Absorption spectrum of $TiO_2$ nanorods only.

induced charge transfer in the MEH-PPV/$TiO_2$-nanorod hybrid materials are investigated by stead-state and time-resolved photoluminescence (PL) spectroscopy and photoluminescence excitation (PLE) spectroscopy. Finally, the current–voltage characteristic of a photovoltaic device based on the MEH-PPV/$TiO_2$ nanorod hybrid material is also reported.

## 2. Experimental methods

The controlled growth of high-aspect-ratio anatase titanium dioxide nanorods were synthesized by the hydrolysis of titanium tetraisopropoxide according to the literature [10]. Typically, oleic acid (120 g, Aldrich, 90%) was stirred vigorously at 120 °C for 1 h in a three-neck flask under Ar flow, then allowed to cool to 90 °C and maintained at this temperature. Titanium isopropoxide (17 mmol, Aldrich, 99.999%) was then added into the flask. After stirring for 5 min, trimethylamine-*N*-oxide dihydrate (34 mmol, ACROS, 98%) in 17 ml of water was injected rapidly. The trimethylamine-N-oxide dihydrate was used as a catalyst for polycondensation. The reaction was continued for several hours to have complete hydrolysis and crystallization. Finally, $TiO_2$ nanorods were obtained with a size of about 4 nm in diameter and 20–40 nm in length. The product was washed and precipitated by ethanol repeatedly to remove residual surfactant. Subsequently, the $TiO_2$ nanorods were collected by centrifugation and then re-dispersed in chloroform or toluene. In the preparation of hybrid materials, the MEH-PPV solution was prepared by dissolving MEH-PPV (Aldrich, USA) in chloroform. Solutions of hybrid materials with 0, 40 and 80 wt% $TiO_2$ were obtained by mixing the required amount of $TiO_2$ nanorod solution with the MEH-PPV solution. Thin-film samples of hybrid material were prepared by spin coating the hybrid solution on silicon substrates and further annealed in vacuum before measurements.

UV–visible absorption spectra were obtained using an Ocean Optics HR-4000 spectrometer. The steady-state PL spectra were measured by using a Perkin-Elmer FS-55 spectrofluorometer. Time-resolved photoluminescence spectroscopy was performed with a time-correlated single photon counting (TCSPC) spectrometer (Picoquant Inc.). A

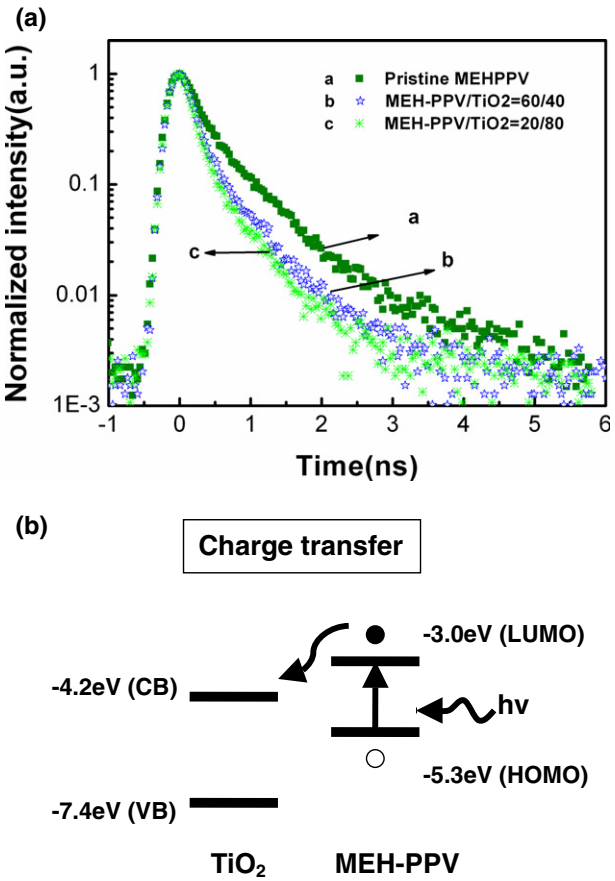


**Figure 3.** (a) Photoluminescence lifetime decay of theses samples at room temperature. The lifetime $\tau_{PL}$ for the pristine MEH-PPV and the composites containing 40 and 80 wt% $TiO_2$ nanorods are 738, 520 and 497 ps, respectively, by a bi-exponential fitting. (b) Schematic representation of charge transfer at the MEH-PPV/$TiO_2$-nanorod interfaces. The vacuum level is defined at 0 eV.

pulse laser (375 nm) with an average power of 1 mW operating at 40 MHz with a duration of 70 ps was used for excitation.

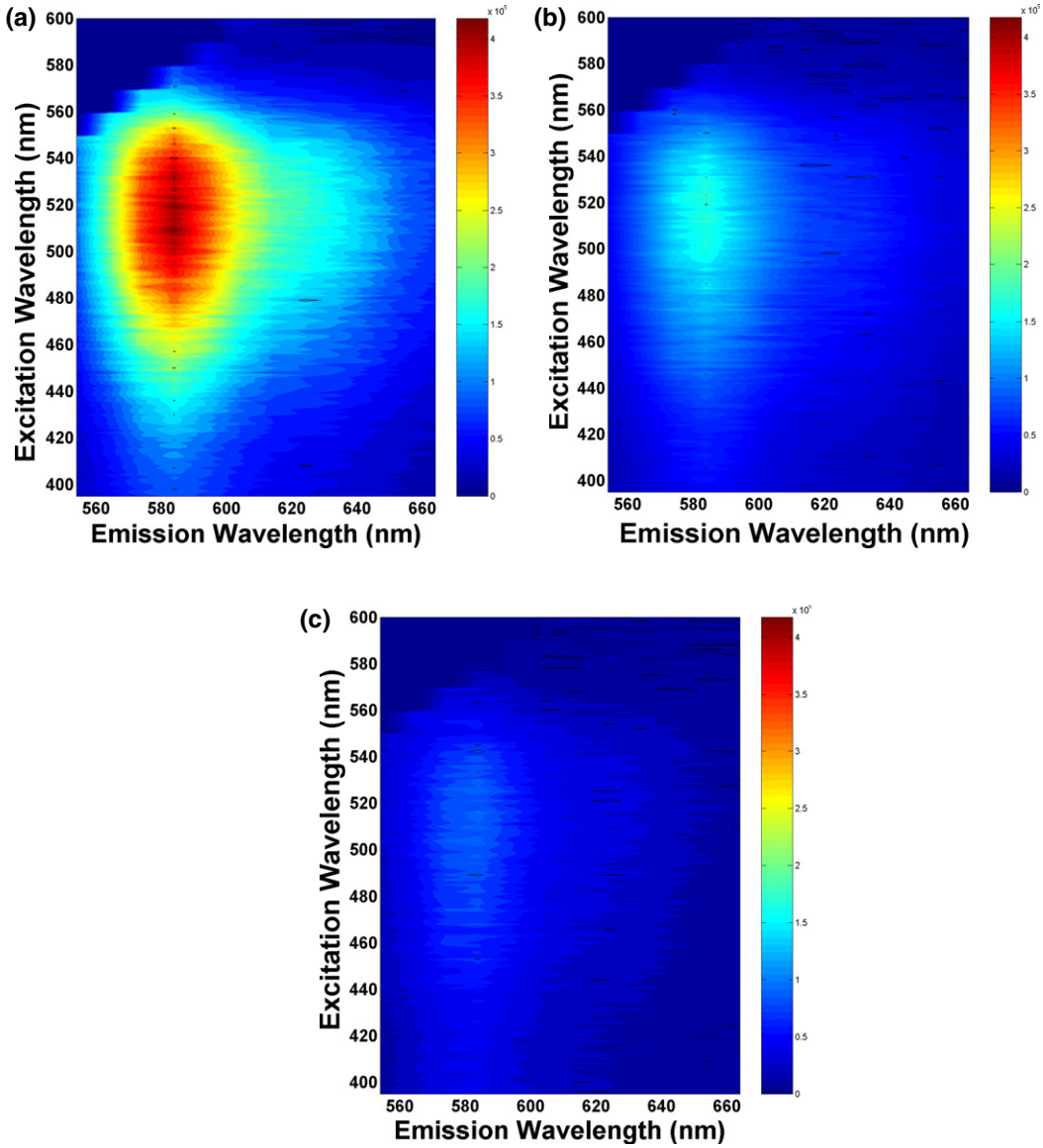


**Figure 4.** Two-dimensional contour plots of the photoluminescence mapping as a function of emission and excitation wavelengths for composite films with (a) 0 wt%, (b) 40 wt%, and (c) 80 wt% of $TiO_2$ nanorod concentrations. To avoid the second-harmonic effect, detection of the emission wavelength is limited to less than twice the excitation wavelength.

During the temperature-dependent PL measurements, the samples were maintained under vacuum inside a helium cryostat, allowing temperature variation between 10 K and ambient temperature. PLE spectroscopy was measured using a FluoroLog®-3 spectrofluorometer (Jobin-Yvon). Film thickness was measured by means of a Veeco M6 surface profiler. Current–voltage characterizations (Keithley 2400 source meter) were performed under a $10^{-3}$ Torr vacuum and under monochromatic illumination at a defined beam size (Oriel Inc.).

## 3. Results and discussions

In this study, $TiO_2$ nanorods of 20–40 nm in length and 4–5 nm in diameter are used. Figure 1 shows transmission electron microscopy (TEM) images of the $TiO_2$ nanorods before being blended with MEH-PPV. Figure 2(a) shows the room-temperature UV–visible absorption and PL spectra of the various blends of MEH-PPV with 0, 40, and 80 wt% of $TiO_2$ nanorods, respectively. To avoid thickness and geometry effects, the optical density of absorption and PL intensity was measured in solution within cuvette cells. The pristine MEH-PPV exhibits a broad absorption spectrum peaked at about 490 nm and $TiO_2$ nanorods have a sharp absorption edge at about 350 nm. As the concentration of the $TiO_2$ nanorods increases, the optical density of the absorption spectra in the composites is simply the sum of the absorption spectra of constituent parts. No evidence of any additional absorption peaks in the measured spectral range is found. With excitation at 450 nm, only the polymer is excited and the PL spectra of the composites show similar emission features with respect to that of the pristine MEH-PPV, indicating that

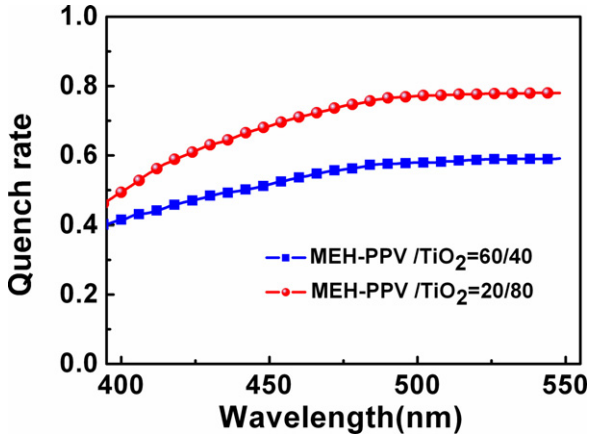


**Figure 5.** The quenching efficiency $Q(\lambda)$ as a function of excitation wavelengths for the composites with respect to pristine MEH-PPV.

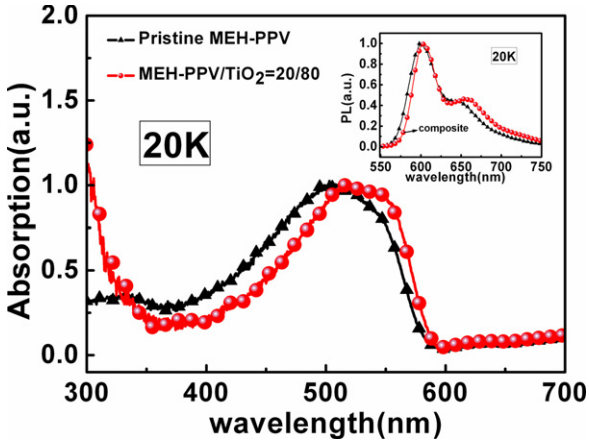


**Figure 6.** Normalized absorption spectra measured at 20 K of the pristine MEH-PPV and the composite film with 80 wt% of $TiO_2$ nanorods. The inset exhibits the normalized PL spectra for the composite and pristine MEH-PPV measured at 20 K.

the luminescence predominantly results from excitons which radiatively recombine in polymer. However, the yield of the PL emission in the composites decreases substantially with increasing $TiO_2$ nanorod content, indicating that charge separation occurs at the interface between the two materials. This produces a charge-separated state with an electron on the $TiO_2$ nanorod and a hole on the polymer, which is responsible for the polymer emission quenching. Figure 3(a) presents the PL decay spectroscopy for the hybrid materials measured at 550 nm. The PL decay in the composite materials demonstrates a monotonic decrease in lifetime with increasing $TiO_2$ nanorod content. The measured lifetime of the luminescence $\tau_{PL}$ can be related to the rate constants for radiative and non-radiative decays, $k_R$ and $k_{NR}$, by $1/\tau_{PL} = k_R + k_{NR}$. The PL efficiency $\eta$ is then given by $\eta = f\frac{k_R}{k_R+k_{NR}} = f(\tau_{PL}/\tau_R)$, where $f$ is the fraction of absorbed photons generating the emissive species and $\tau_R = 1/k_R$ is the natural radiative lifetime, i.e. the lifetime that the luminescence would have in the absence of a competing non-radiative decay process. As the $TiO_2$ nanorod concentration increases, a new relaxation process is present, which provides to the donor a further non-radiative process, leading to the enhancement of the non-radiative decay rate $k_{NR}$. This leads to a shortening of the measured lifetime $\tau_{PL}$ and quenching of the PL efficiency $\eta$. Figure 3(b) exhibits schematically the mechanism of charge transfer at the MEH-PPV/TiO2-nanorod interfaces. By taking the PL efficiency of the pristine MEH-PPV as 100% and the natural radiative lifetime as $\tau_0$ for reference, the *relative* natural radiative lifetime $\tau_R$ for the composites calculated according to $\eta = f(\tau_{PL}/\tau_R)$ can be estimated to be about $1.09\tau_0$ and $1.12\tau_0$ for the samples containing 40 and 80 wt% nanorods, respectively. The increase in natural radiative lifetime, $\tau_R$, for the composites with respect to the pristine MEH-PPV implies that the excitons, which contribute to the remaining luminescence by radiative recombination in the polymer, will migrate along the polymer chains over a larger region before recombination.

The two-dimensional PL contour plots of the composite thin films with 0, 40, and 80 wt% of $TiO_2$ nanorod concentrations as a function of emission and excitation wavelengths are shown in figures 4(a)–(c), respectively. The excitation wavelengths were chosen to keep the condition that only the polymer absorbs the light intensity. These samples are prepared by spin-coating the mixture of MEH-PPV and $TiO_2$ nanorods onto Si substrates. The film thickness for these samples was about 120 ± 10 nm. For the pristine MEH-PPV, the PL maxima (spots) on the map in figure 4(a) are clearly seen at about 570–590 nm, consistent with the PL emission peak in figure 2(a). As the concentrations of $TiO_2$ nanorods are increased up to 40 and 80 wt%, as shown in figures 4(b) and (c) respectively, the intensities of the PLE signals quench at all emission wavelengths, indicating that efficient charge separation occurs at the $TiO_2$-nanorod/MEH-PPV interfaces. Figure 5 shows the quenching efficiency $Q(\lambda)$ as a function of excitation wavelength from 400 to 550 nm for the composites with respect to pristine MEH-PPV. The quenching rate is enhanced with increasing $TiO_2$ nanorod content in the composite films. For excitation with a longer wavelength closer to the PL emission peak, the quench rate is also increased. In addition, it is worth noting that the fluorescence quenching for the composite thin films is more efficient with respect to the mixed solutions in our case. Similar observation has also been reported previously [7, 11], where the possible formation of nanocrystal aggregation may take place in solutions or thicker films.

We have further characterized the optical properties of the composite films at low temperature. Figure 6(a) shows the absorption spectra of pristine MEH-PPV and the composite film with a 80 wt% $TiO_2$ nanorod concentration, respectively, measured at 20 K. As shown in figure 2(a), a similar absorption peak at about 500 nm is observed for these two samples. As the temperature is lowered to 20 K, there is a significant red-shift in the absorption spectrum for the composite film with respect to pristine MEH-PPV. The effective conjugation length in polymer chains increases with decreasing temperature, owing to the reduction in thermal disorder. Accordingly, enhancement in the delocalization of the $\pi$-electrons brings the absorption peaks to lower energies as the temperature is lowered [12]. For the composite film, a larger red-shift in the absorption peak at low temperature with respect to pristine MEH-PPV indicates that the inclusion of $TiO_2$ nanorods

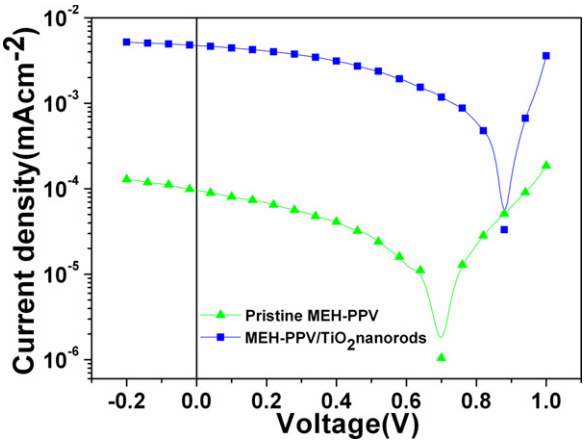


**Figure 7.** Current–voltage curve for a device containing 54 wt% $TiO_2$ nanorods in the dark (triangles) and under illumination (squares) at 450 nm. The power density of illumination is about 0.5 W $m^{-2}$.

in the polymer can further reduce disorder in conformation and enhance conjugation in the polymer chains. A red-shift in the normalized PL spectrum for the composite film with respect to that of pristine MEH-PPV is also shown in the inset. Similar observation in the poly(3-octylthiophene) consisting of thiophene rings having large alkyl groups [13] and in MEHP-PPV/CdSe-nanoparticle composite films [14] has also been reported. Rapid charge separation at the $TiO_2$-nanorod/polymer interfaces leads to efficient exciton dissociation, showing quenching of the PL efficiency and shortening of the PL lifetime. The surviving excitons that contribute to the remaining luminescence in the polymer will migrate over more conjugated polymer chains, formed by the more rigid structures owing to the inclusion of $TiO_2$ nanorods in the host polymer. The result is also consistent with the increase in natural radiative lifetime, $\tau_R$, for the composites with respect to pristine MEH-PPV, as mentioned above.

Figure 7 shows the current–voltage curves of two solar cell devices consisting of pristine MEH-PPV and a hybrid MEH-PPV/$TiO_2$-nanorod layer with a similar thickness under monochromatic illumination at 450 nm, respectively. The devices are fabricated with an active layer sandwiched between electrodes of indium tin oxide (ITO) and aluminium. The composite material consists of 54 wt% $TiO_2$ nanorods. An increase in the photocurrent $J_{sc}$ (at 0 V bias) of about two orders of magnitude is found for the device containing the MEH-PPV/$TiO_2$-nanorod composite compared to that with pristine MEH-PPV, indicating that efficient charge separation is taking place at the MEH-PPV/$TiO_2$-nanorod interfaces.

## 4. Conclusion

In conclusion, the mechanisms of photoinduced charge transfer in $TiO_2$-nanorod/MEH-PPV composites are investigated. Efficient charge transfer takes place at the $TiO_2$-nanorod/polymer interfaces when the polymer is excited, leading to quenching of the PL intensity and shortening of the measured lifetime. The excitons that contribute to the remaining luminescence in the polymer migrate over more conjugated polymer chains, formed by the more rigid structures owing to the inclusion of $TiO_2$ nanorods in the host polymer. Efficient charge separation at $TiO_2$-nanorod/MEH-PPV interfaces indicates that the composite will be a good candidate for photovoltaic applications.

## Acknowledgments

This work is supported by the National Science Council, Taiwan (project no. NSC94-2120-M-002-010) and the US Airforce project.

## References

[1] Huynh W U, Dittmer J J and Alivisatos A P 2002 *Science* **295** 2425
[2] Ma W, Yang C, Gong X, Lee K and Heeger A J 2005 *Adv. Funct. Mater.* **15** 1617
[3] Yu G and Heeger A J 2001 *J. Appl. Phys.* **78** 4510
[4] Haugeneder A, Neges M, Kallinger C, Spirkl W, Lemmer U and Felmann J 1999 *Phys. Rev.* B **59** 15346
[5] Dittmer J *et al* 2000 *Sol. Energy Mater. Sol. Cells* **61** 53
[6] Dittmer J J, Marseglia E A and Friend R H 2000 *Adv. Mater.* **12** 1270
[7] Greenham N C, Peng X and Alivisatos A P 1996 *Phys. Rev.* B **54** 17628
[8] Hagfeldt A and Grätzel M 2000 *Acc. Chem. Res.* **33** 269
[9] Ravirajan P, Bradley D D C, Nelson J, Haque S A, Durrant J R, Smit H J P and Kroon J M 2005 *Appl. Phys. Lett.* **86** 143101
[10] Cozzoli P D, Kornowski A and Weller H 2003 *J. Am. Chem. Soc.* **125** 14539
[11] Petrella A, Tamborra M, Curri M L, Cosma P, Striccoli M, Cozzoli P D and Agostiano A 2005 *J. Phys. Chem.* B **109** 1554
[12] Hagler T W, Pakbaz K, Voss K F and Heeger A J 1991 *Phys. Rev.* B **44** 8652
[13] Watanabe A, Kodaira T and Ito O 1997 *Chem. Phys. Lett.* **273** 227
[14] Lin Y Y, Chen C W, Chang J, Lin T Y, Liu I S and Su W F 2006 *Nanotechnology* **17** 1260